Phosphorylation control of p53 DNA binding cooperativity balances tumorigenesis and aging

Oleg Timofeev[1], Lukas Koch[1], Constantin Niederau[1], Alina Tscherne[1], Jean Schneikert[1], Maria Klimovich[1], Sabrina Elmshäuser[1], Marie Zeitlinger[1], Marco Mernberger[1], Andrea Nist[2], Christian Osterburg[3], Volker Dötsch[3], German Mouse Clinic Consortium[§], Martin Hrabé de Angelis[4,5,6], and Thorsten Stiewe[1,2]

[1] Institute of Molecular Oncology, Member of the German Center for Lung Research (DZL), Philipps-University, Marburg, Germany;
[2] Genomics Core Facility, Philipps-University, Marburg, Germany;
[3] Institute of Biophysical Chemistry, Goethe University, Frankfurt, Germany;
[4] German Mouse Clinic, Institute of Experimental Genetics, Helmholtz Zentrum München, German Research Center for Environmental Health, Neuherberg, Germany
[5] Chair of Experimental Genetics, School of Life Science Weihenstephan, Technische Universität München, Freising, Germany;
[6] German Center for Diabetes Research (DZD), Neuherberg, Germany;
[§] Full list of authors and their affiliations appears at the end of the paper;
Martin Hrabé de Angelis and Thorsten Stiewe contributed equally to this work

Running title: p53 phosphorylation balances tumorigenesis and aging

Corresponding authors:
Oleg Timofeev, Institute of Molecular Oncology, Philipps-University Marburg, Hans-Meerwein-Str. 3, 35043 Marburg, Germany; phone: +49 6421 26 66768, email: timofeev@staff.uni-marburg.de.
Thorsten Stiewe, Institute of Molecular Oncology, Philipps-University Marburg, Hans-Meerwein-Str. 3, 35043 Marburg, Germany; phone: +49 6421 28 26280; email: stiewe@uni-marburg.de.

The authors declare no potential conflicts of interest.

Abstract

Post-translational modifications are essential for regulating the transcription factor p53 which binds DNA in a highly cooperative manner to control expression of a plethora of tumor suppressive programs. Here we show at the biochemical, cellular, and organismal level that the cooperative nature of DNA binding is reduced by phosphorylation of highly conserved serine residues (human S183/S185, mouse S180) in the DNA binding domain. To explore the role of this inhibitory phosphorylation in vivo, new phosphorylation-deficient p53-S180A knock-in mice were generated. ChIP-seq and RNA-seq studies of S180A knock-in cells demonstrated enhanced DNA binding and increased target gene expression. In vivo, this translated into a tissue-specific vulnerability of the bone marrow that caused depletion of hematopoietic stem cells and impaired proper regeneration of hematopoiesis after DNA damage. Median lifespan was significantly reduced by 20% from 709 days in wild-type to only 568 days in S180A littermates. Importantly, lifespan was reduced by a loss of general fitness and increased susceptibility to age-related diseases, not by increased cancer incidence as often seen in other p53 mutant mouse models. For example, S180A knock-in mice showed markedly reduced spontaneous tumorigenesis and increased resistance to *Myc*-driven lymphoma and *Eml4-Alk*-driven lung cancer. Preventing phosphorylation of S183/S185 in human cells boosted p53 activity and allowed tumor cells to be killed more efficiently. Together out data identify p53 DNA binding domain phosphorylation as a druggable mechanism that balances tumorigenesis and aging.

Significance: Findings demonstrate that p53 tumor suppressor activity is reduced by DNA binding domain phosphorylation to prevent aging and identify this phosphorylation as a potential target for cancer therapy.

Introduction

TP53 is arguably the most powerful tumor suppressor that governs a plethora of cellular programs, some of which can support survival and provide recovery of the cell after damage, whereas others lead to cell death. As a transcription factor, p53 controls expression of hundreds of genes, creating a sophisticated regulatory network which requires a tight regulation of p53 itself. Complex patterns of post-translational modifications (PTM) under basal conditions or upon stress determine subcellular localization, transcriptional activity and stability of the p53 protein (1). Multiple phosphorylation sites, involved in the regulation of p53's stability, transcriptional activity and non-transcriptional functions were identified in the N- and C-terminal domains (1). In addition, several important modifications, such as Lys^{120} and Lys^{164} acetylation, which enhance transactivation and induction of p53-dependent apoptosis, were mapped to the DNA-binding domain (DBD) (2-4). The functional significance of other PTMs in the DBD is less well established. Phosphorylation of the DBD residues Ser^{183}, Thr^{211} and Ser^{215} by Aurora B kinase was shown to promote p53 degradation via the ubiquitin-dependent proteasomal pathway (5). Similarly, Ser^{183}, Ser^{269} and Thr^{284} were identified as Aurora B kinase phosphorylation sites that inhibit the transcriptional activity of p53 (6). Moreover, extensive mass spectrometry analyses confirmed these and Ser^{185} as a novel DBD phosphorylation site (7,8). Whether and how these DBD phosphorylation events affect DNA binding remains unclear.

p53 binds DNA as a tetramer in a sequence-specific manner. Its prototypical response element (RE) consists of two decameric RRRCWWGYYY half-sites (where R=A,G; W=A,T; Y=C,T) separated by a facultative spacer of 1-21 bases (9). The binding by four monomers is cooperative and the degree of cooperativity determined by structural properties encoded in the RE base sequence (10,11). p53 binds with high affinity and low cooperativity to REs with a central CATG sequence that possess a high

torsional flexibility, whereas binding to more rigid CAAG, CTTG and CTAG REs, frequently found in promoters of pro-apoptotic target genes, occurs with a high degree of cooperativity (9,11,12). DNA binding cooperativity therefore differs within the p53 cistrome and distinguishes, for instance, p53's pro-apoptotic and apoptosis-independent functions (13-16). Cooperative DNA binding is structurally not only supported by p53's dedicated tetramerization domain, but also by interactions between neighboring DNA binding core domains, in particular by reciprocal salt bridges formed by the oppositely charged amino acids Glu^{180} and Arg^{181} of the short H1 helix (17-20). A reduction in cooperativity dramatically affects sequence-specific DNA binding of p53 and disturbs its physiological functions *in vivo* (13-16,21). For example, the cooperativity-reducing mutation E180R leads to loss of binding to pro-apoptotic gene promoters, causing a selective defect in DNA damage-triggered apoptosis and compromised tumor suppression (15), whereas the R181E substitution has an even more pronounced effect on DNA binding and abolishes the transcriptional activity completely (14,16). It is therefore not surprising that cooperativity-reducing Glu^{180} and Arg^{181} mutations form a mechanistically distinct class of tumor-associated p53 mutations found in an estimated number of 34,000 cancer patients per year worldwide (16,22).

The phosphorylation sites Ser^{183} (S183) and Ser^{185} (S185) are located in direct vicinity to the H1 helix salt bridge residues, tempting us to speculate that phosphorylation of these serine residues may affect DNA binding cooperativity and represent a mechanism for controlling DNA binding-dependent p53 functions.

Materials and Methods

Animal experiments

The B6.129S/Sv-*Trp53*^{tm3Thst} knock-in mouse with the conditional *Trp53*^{LSL}-S180A (TCC>GCC) mutation was generated by Ingenious Targeting Laboratory as described (15). *Trp53*$^{+/LSL-S180A}$ mice were crossed with 129S/Sv-Tg(Prm-cre)58Og/J animals to obtain *Trp53*$^{+/S180A}$ mice, which were intercrossed to generate homozygous animals and wild-type mice as littermate controls. *Trp53*^{LSL}-S180A/LSL-S180A mice were used as p53-negative controls.

For generation of B-cell lymphoma, *Trp53*$^{+/S180A}$ females were crossed with B6.Cg-Tg(IghMyc)22Bri/J males (23). For somatic CRISPR-induced lung mutagenesis (24), we used age- and gender-matched *Trp53*$^{S180/S180A}$ and wild-type littermates carrying a floxed luciferase reporter (B6.129-*Gt(ROSA)26Sor*$^{tm2(ACTB-Luc)Tyj}$/Nci) to monitor lung tumorigenesis by bioluminescence imaging (BLI). Recombinant CRISPR-adenovirus ($1x10^{10}$ – $5x10^{10}$ PFU) was delivered intratracheally as described (25). Mouse imaging was performed using the In Vivo Xtreme II System (Brucker), 7T Clinscan 70/30 USR (Brucker) or computer tomograph nanoScan PET-CT (Mediso).

For studying acute DNA damage responses, mice were subjected to an X-ray dose of 6 Gy (1 Gy/minute) using an X-RAD 320iX (Precision X-Ray) irradiator. In muscle regeneration experiments mice of both genders were used as described (26,27).

A cohort of 57 littermates, 15 mutant males and 15 control males, 14 mutant females and 13 control females, were phenotypically analyzed at the German Mouse Clinic (GMC) at the age of 8 to 19 weeks. The standardized screening pipeline for systematic primary phenotyping was previously described (28). Mouse phenotyping methods were reported before (29-31).

All mouse experiments were performed according to the German Animal Welfare Law (TierSchG). At the GMC, mice were maintained in IVC cages with water and standard mouse chow according to the GMC housing conditions; all tests performed were approved by the responsible authority of the district government of Upper Bavaria, Germany. Mouse experiments at Philipps-University Marburg, were approved by the Regierungspräsidium Giessen, Germany.

Cell culture, plasmids and viruses

HCT116, H1299 and Saos-2 cell lines were obtained directly from the ATCC (LGC Standards), authenticated in the experiments by p53 genotyping and tested negative monthly for mycoplasma as described (32). Primary MEFs, thymocytes and splenocytes were isolated and maintained as described (16). Transfections and viral infections were performed as described (15). For recombinant protein expression in E. coli, thermostable p53 (p53TS) constructs (amino acid 41 to 356; M133L/V203A/N239Y/N268D) (33,34) were cloned into a pET-15b expression vector with an N-terminal His_{10}-tag followed by a TEV protease cleavage site. Lentiviruses were produced as described (16). p53 phospho-variants were generated in pENTR/D-TOPO vector (Invitrogen) with human p53 cDNA using QuickChange Multi Site-Directed Mutagenesis Kit (Agilent) and mutagenesis oligonucleotides listed in Supplementary Table S1. p53 variants were shuttled into pInducer20 and pAdEasy-CMV-Flag (Agilent) vectors using the Gateway® System (Invitrogen). pAd-Cas9-Eml4-Alk (24) and pAd-Cas9-Cre-Eml4-Alk (derived from pAd-Cas9-Eml4-Alk by insertion of a Cre-T2A fragment upstream of the FLAG-Cas9 sequence) constructs were used for generation of adenovirus in Ad293 cells (Agilent) as described (13).

Thermal Shift Assay (TSA)

TSA was performed to record melting curves with an iCycler iQ PCR Thermal Cycler (Bio-Rad). Proteins were diluted with SEC Buffer to a concentration of 35 µM. 36 µl diluted protein solution was mixed with 4 µl SYPRO Orange dye (Thermo Fisher) diluted 1:200 in SEC Buffer. Samples were transferred into MicroAmp Optical 96-well plates (Thermo Fisher) and measured every 0.2°C from 22°C to 90°C with an increase of 1°C/min. The first deviation of the fluorescence signal was normalized and plotted to extract the melting point.

Plasmon Surface Resonance (SPR)

DNA binding was measured with the Biacore X-100 system (GE Healthcare) as previously described for the p63 DBD (35). All assays were performed at 20°C and in a modified HBS-P buffer (25 mM HEPES pH7.5, 200 mM NaCl, 0.5 mM TCEP, 0.005% Surfactant P-20). Biotin-labeled 20bp double-stranded DNA oligonucleotides (Supplementary Table S1) were prepared annealing the biotinylated forward strand including a T11 tether in a 1:4 ratio with its respective reverse strand. DNA was captured on the streptavidin (SA) coated sensor chip (GE Healthcare) in the respective flow cells until reaching ~100 response units (RU). Measurements were performed with a flow rate of 10 µl/min and included three start-up injections followed by up to 14 injections of p53 with increasing concentrations. Each injection lasted 3 min followed by a 3 min dissociation phase and two injections of regeneration buffer. Data was evaluated using the BIAevaluation software (GE Healthcare) and Prism 8 (GraphPad).

Electrophoretic mobility shift assay (EMSA) and luciferase reporter assays

For EMSA, [γ-^{32}P]-labeled DNA oligonucleotide (Supplementary Table S1), 5 µl of in vitro translated protein, 100 ng α-p53 antibody (Pab421) and 10 pmol unlabeled scrambled oligo were incubated in a total volume of 20 µl of EMSA buffer (20 mM

HEPES pH 7.8, 0.5 mM EDTA, 6 mM $MgCl_2$, 60 mM KCl, 0.008% Nonidet P-40, 1 mM DTT, 5% glycerol) supplemented with 120 ng salmon sperm DNA as described (13). For luciferase assay, H1299 cells were co-transfected with 200 ng pGL3 reporter plasmid containing a p53 response element, 50 ng phRL-TK plasmid encoding Renilla luciferase for normalization and 100-150 ng p53 expression plasmids (pInducer20); the total amount of DNA per transfection was equalized to 500 ng by addition of pUC19 plasmid. Expression of p53 was induced upon addition of 0.001-0.01 μg/ml doxycycline 6 h after transfection. 24 h after transfection, luciferase activities were measured with D-luciferin or coelenterazine using Orion II Microplate Luminometer (Titertek).

CRISPR/Cas9 gene editing

HCT116 *TP53*$^{+/-}$ cells were co-transfected with pX330 (Addgene plasmid #42230) encoding *TP53*-intron5-specific sgRNA and a custom-synthesized (Thermo Fischer Scientific) donor DNA for homology-directed repair containing 1600 bp *TP53* gene sequence (GRCh38/hg38 chr17:7.676.100-7.674.500) with the mutations S183A;S185A (chr.17:7.675.063-7.675.065; chr.17:7.675.057-7.675.059). Transfected cells were expanded as single-cell clones and analyzed by PCR and Sanger sequencing for correct recombination.

Flow cytometry

Bone marrow samples for flow cytometry were collected as described (36) and 1 million cells were resuspended in 100 μl MACS buffer (0.5% BSA, 2 mM EDTA in PBS pH7.2) for staining with: biotin-AB Lin cocktail and streptavidin APC-Cy7 (Miltenyi Biotech), FITC CD117 (c-Kit) (Biolegend #105805), PE-Cy5 Sca1 (Ly-6A/E) (Biolegend #108109), BV 421™ CD135 (Flk2) (BLD-135313), PE/Dazzle™ 594 CD34

(BLD-128615). Staining was done as described (16) and analyzed using LSRII (BD) cytometer and FlowJo (BD) software. Apoptosis, cell viability and cell cycle profile were analyzed as described (16).

Immunohistochemistry, immunofluorescence and western blot

Sample preparation, immunoblotting, immunofluorescence and immunohistochemistry were performed as described (15) using: mouse p53 (NCL-p53-505, Leica Microsystems, 1:2000), human p53 (DO-1, Santa Cruz Biotechnology [SC], 1:2000), p53 phospho-Ser15 (#9284, Cell Signaling, 1:100), cleaved caspase-3 (#9661, Cell Signaling, 1:500), cleaved PARP (#9541, Cell Signaling, 1:500), p21 (WB: F-5, #sc-6246, SC, 1:200; IHC: #ab188224, Abcam, 1:1000), BrdU (BU1/75(ICR1), #OBT0030G, 1:100), pErk (E-4, SC, 1:100), anti-Ki-67 (TEC-3, DAKO, 1:100), β-actin (AC-15, #ab6276, Abcam, 1:10000), DeadEnd TM colorimetric TUNEL System (Promega).

ChIP-seq and RNA-seq

Chromatin immunoprecipitation from primary MEFs treated for 16 h with 0.1% DMSO (control) or 10 μM Nutlin-3a (Nutlin) was done as described (16) using anti-p53 antibody (FL393, Santa Cruz) and normal rabbit IgG (Santa Cruz) as the control. ChIP-seq libraries were prepared with the Microplex Library Preparation Kit (Diagenode) according to the manufacturer's instructions. For RNA-seq, RNA quality was assessed using the Experion RNA StdSens Analysis Kit (BioRad), libraries were prepared using the TruSeq Stranded mRNA LT kit (Illumina) according to the manufacturer's instructions, sequenced on the HiSeq 1500 platform (Illumina) in Rapid-Run mode with 50 base single reads and archived at EBI ArrayExpress (E-MTAB-6774, E-MTAB-6793, E-MTAB-9170, E-MTAB-9171).

For ChIP-seq analysis, samples were mapped to the Ensembl Mus musculus reference genome (release 79, GRCm38, mm10) using Bowtie2 (v.2.0.0), aligned reads were deduplicated and subjected to peak calling using MACS (v.1.4) with the sample input as reference. To reduce the number of false positive ChIP-seq peaks, reported peaks were filtered to retain regions with >3-fold enrichment of read counts compared to input, >50 reads in the sample lane and <50 reads in the input. Blacklisted hyper-chipable regions were excluded. Read counts per million were calculated and averaged over all binding sites.

For RNA-seq analysis, reads were mapped as described above and differential expression was assessed using DEseq2 (v.1.14.1). TPMs (Transcripts per Kilobase Million) were calculated and z-transformed values were depicted as heatmaps. Gene set enrichment analysis was performed using the GSEA software (v.2.1.0) and MSigDB database (v.5.0) using genotype permutation (1000 permutations) and the Signal-to-Noise ratio based on TPMs.

Statistical analysis

For statistical analysis we used GraphPad Prism 8 software. If not stated otherwise, data that was generated by the German Mouse Clinic was analyzed using R (Version 3.2.3). Graphs show mean values obtained with n technical or biological replicates, and error bars in all figures represent standard deviation (SD), unless indicated otherwise. Tests for genotype effects were made by using t-tests, Mann-Whitney tests, Chi-square tests or linear models depending on the assumed distribution of the parameter and the questions addressed to the data. Multiple t-testing was performed in combination with the False Discovery Rate (FDR) approach (two-stage linear step-up procedure of Benjamini, Krieger and Yekutieli). p- or FDRq-values <0.05 were used as level of significance.

Results

Phospho-mimic mutations of Ser^{183} and Ser^{185} reduce DNA binding and transcriptional activity

Cancer-associated mutations in *TP53* most frequently affect codons that are highly conserved in evolution. Notably, mammalian *TP53* encodes conserved serines next to the H1 helix salt-bridge residues E180 and R181 (Fig. 1A). While S185 is missing in rodents, S183 is present in almost all mammals. Nevertheless, cancer-associated mutations that affect codons S183 and S185 of human *TP53* are remarkably rare (Fig. 1B). Although there are 35 cases of S183/S185 nonsense or frameshift mutations, there is not a single S183/S185 missense mutation among the 47,005 tumor samples in a curated set of non-redundant TCGA studies (37), suggesting no tumor-promoting activity of missense mutations at these codons. This is supported also by the UMD and IARC *TP53* mutation databases: whereas 72.8% of all *TP53* mutations are missense mutations, S183 mutations are nonsense or frameshift mutations in 86.2% (UMD) and 81.1% (IARC). In detail, the UMD database comprises 58,517 *TP53* missense mutations but lists only 18 S183 and 25 S185 missense mutations, yielding a residue-specific mutation frequency of 0.031% and 0.043%, respectively. Likewise, the IARC *TP53* Database for 21,781 cases of somatic *TP53* missense mutations contains records on 9 missense mutations affecting codon S183 (0.041%) and 22 mutations at codon S185 (0.087%). These mutation frequencies are approximately 100-fold lower than codon 175 missense mutations (UMD: 6.3%; IARC: 6.1%) and almost 3 to 8-fold lower than expected by chance (0.25%). The striking underrepresentation of missense mutations at S183/S185, despite evolutionary conservation of these codons, suggested that loss of these serine residues does not promote transformation and is possibly even detrimental for tumorigenesis.

Since serine phosphorylation sets a negative charge and has been shown to weaken nearby salt bridges in other proteins (38), we reasoned that it could affect the critical electrostatic interactions between H1 helices and thereby reduce DNA binding cooperativity. We expressed and purified thermostable p53 (amino acid 41-356) with phospho-mimic (S>D) or phospho-deficient (S>A) mutations and the R273H mutant as a negative control (Supplementary Fig. S1A). The melting temperature of the purified proteins was only marginally changed (Fig. 1C,D), suggesting that S183/S185 phospho-mutations do not change protein folding like many classical tumorigenic mutations that strongly destabilize the structure of the DBD . Measurement of the binding affinity of purified proteins to a p53 response element in the *CDKN1A*/p21 promoter by surface plasmon resonance detected a slightly, but significantly reduced affinity for the phospho-mimic S183D/S185D (DD) variant, whereas the phospho-deficient S183A/S185A (AA) variant showed a K_D similar to wild-type p53 (Fig. 1E,F, Supplementary Fig. S1B).

Next, full-length p53 cDNA constructs with various single and double phospho-mimic (S>D or S>E) or phospho-deficient (S>A) codon 183 and 185 point mutations. were used for electrophoretic mobility shift assays with oligonucleotides containing high and low affinity p53 response elements (Fig. 1G, Supplementary Fig. S1C). The binding of phospho-deficient variants were similar to the wild-type p53 protein. Contrarily, phospho-mimic mutations only slightly affected binding to response elements with a CATG half site, but strongly reduced binding to CAAG and CTAG half sites, which are bound by wild-type p53 with high cooperativity (11). The same was previously observed when studying cooperativity mutations affecting residues E180 and R181 (13,39), supporting the idea that phosphorylation of S183 and S185 reduces DNA binding cooperativity similar to salt bridge mutations.

To analyze how S183/S185 phosphorylation affects transcriptional activity, we examined different phospho-variants in a luciferase reporter assay (Fig. 1H, Supplementary Fig. S1D). Consistent with *in vitro* DNA binding assays, the DD variant displayed the lowest transcriptional activity for all tested response elements, whereas the AA variant was transcriptionally at least as efficient as the wild-type protein (Fig. 1H). Importantly, the difference between DD and AA variants was the greatest for reporter constructs containing low affinity response elements of pro-apoptotic targets *TP53AIP1* and *BAX* that are bound by wild-type p53 with high cooperativity (Fig. 1H, Supplementary Fig. S1D). Taken together, our data demonstrate for S183/S185 phospho-mimic variants a phenotype remarkably similar to E180/R181 cooperativity mutants, suggesting that phosphorylation of serines adjacent to the H1 helix salt bridge reduces DNA binding cooperativity, resulting in decreased DNA binding and transcriptional activity.

Phospho-deficient S180A variant displays increased transcriptional activity

S183 from human p53 is conserved in the mouse and corresponds to S180 (Fig. 1A). To examine whether constitutive removal of this phosphorylation would affect p53 activity *in vivo*, we generated a phospho-deficient *Trp53*^{S180A} (S180A, short SA) knock-in mouse (Supplementary Fig. S2). Homozygous knock-in embryos developed normally. p53 chromatin immunoprecipitation coupled with next generation sequencing (ChIP-seq) in DMSO- or Nutlin-treated p53$^{+/+}$ and homozygous S180A mouse embryonic fibroblasts (MEFs) revealed a significant enrichment of the canonical p53 binding motif in both genotypes, but the strength of binding was markedly increased in phosphorylation-deficient cells – especially at sites that were only weakly bound by wild-type p53 (Fig. 2A-C). When comparing the sequences of peaks strongly bound by p53 in both wild-type and knock-in cells to the peaks showing the strongest binding

difference between both genotypes, the latter were significantly enriched in sequences that deviate from the canonical p53 binding site and were previously shown to require cooperativity for efficient binding (Fig. 2D) (11,13,14,39). In parallel, we analyzed the p53-dependent transcriptome using RNA-seq. In line with the ChIP-seq data, gene set enrichment analysis (GSEA) did not only reveal robust activation of p53 target gene sets in both wild-type and knock-in cells, but also a small but significant increase in the expression of various curated sets of p53 target genes in S180A as compared to wild-type cells (Fig. 2E-F). Furthermore, when Nutlin-activated genes with a binding site in the ChIP-seq dataset were divided into two equal-sized groups with strong (top 50%) versus weak (bottom 50%) binding of p53 (Fig. 2G), the average expression in the top was significantly higher than in the bottom for both genotypes, confirming that transactivation correlates with binding intensity (Fig. 2H). Of note, expression was significantly higher in S180A than WT MEFs for genes with both strong and weak ChIP-seq signasl (Fig. 2H), highlighting that the S180A mutation is globally increasing target gene expression.

S180A MEFs have reduced proliferative potential and are senescence-prone

We next explored the impact of the S180A variant at the cellular level. Upon γ-irradiation (IR), MEFs of both genotypes showed a similar and transient p53 stabilization (Fig. 3A). Induction of target genes was indistinguishable at earlier time points and only slightly increased in some S180A MEFs at 48 hours (Fig. 3B), suggesting a minor role of S180 phosphorylation in this setting. Likewise, thymocytes or splenocytes of both genotypes showed similar dynamics of cell death when irradiated *ex vivo* (Fig. 3C,D).

However, we noted that proliferation of primary S180A embryonic fibroblasts was already exhausted after the second passage, whereas WT cells continued to divide at

least 2-3 passages longer (Fig. 3E). In line with p53-dependent senescence triggered by unphysiologically high ambient oxygen levels (40), proliferation of WT MEFs was completely rescued at physiological levels of 3% oxygen (Fig. 3E). In contrast, the proliferative potential of S180A cells was extended but eventually still exhausted, suggesting an increased sensitivity to persistent low-level oxidative stress in cell culture. Consistently, also treatment with low doses of doxorubicin, which activates p53 in a reactive oxygen species (ROS)-dependent manner (41,42), induced a significantly higher number of senescent S180A fibroblasts (Fig. 3F,G), confirming that S180 phosphorylation-deficiency renders MEFs more prone to senescence.

Increased acute stress response in the bone marrow of S180A mice

To explore the *in vivo* response of S180A knock-in mice to acute DNA damage, we subjected mice to whole-body IR. As expected, p53 protein was undetectable under normal conditions (Fig. 4A, Supplementary Fig. 3-5). In irradiated radiosensitive tissues (bone marrow, thymus, spleen, intestine), p53 became quickly stabilized, activated its target gene *Cdkn1a/p21* and rapidly triggered cell death irrespective of genotype (Fig. 4A-C, Supplementary Fig. S3A-D, Fig. S4A,B). Of note, the radio-resistant organs lung, liver and kidney remained apoptosis-free also in S180A mice (Supplementary Fig. S5).

Radiation-induced cell cycle arrest was observed in mice with both genotypes (Fig. 4D, Supplementary Fig. S3E, S4C). In the intestine, proliferation resumed after 48 hours with similar kinetics in both genotypes (Supplementary Fig. S4C). In contrast, at this time point BrdU-positive cells were absent in the thymus and spleen of S180A mice, while first proliferating cells were clearly detectable in WT animals (Supplementary Fig. S3E). Likewise, we observed significantly lower numbers of BrdU-positive cells in S180A versus WT bone marrow samples 72 hours after IR, despite

similar induction of apoptosis (Fig. 4D,E). Together, these differences indicated a higher sensitivity of hematopoietic S180A cells and suggested defects in restoration of hematopoiesis after DNA damage.

We therefore analyzed the hematopoietic compartment in more detail. In the absence of exogenous genotoxic stress S180A mice showed a pronounced reduction in total bone marrow cellularity, which was accompanied by a somewhat increased, but not reduced number of $Lin^{-/low}$, $Sca1^{+}$, $c\text{-}Kit^{+}$ (LSK) hematopoietic stem cells (HSC) and LSK, $CD34^{-}$, $Flk2^{-}$ long-term (LT) HSCs (Fig. 4F; Supplementary Fig. S6A). Together with a slightly reduced proportion of lymphoid and increased percentage of myeloid cells in the peripheral blood of S180A mice (Supplementary Table S2), these data remind of an “aged hematopoietic phenotype” which is characterized by a reduced functionality of long-term stem cells (LT-HSC) (43). To test the regenerative ability of the LT-HSC, we performed myeloablation experiments with 5-fluorouracil (5FU) (44). 5FU eliminates fast proliferating short-term progenitor cells, sparing LT-HSC which survive and ensure recovery of hematopoiesis by replenishing the progenitor pools. As expected, one week after 5FU injection we detected in both groups a marked drop in the blood leukocyte count (Fig. 4G). 12 days after treatment, the number of leukocytes was restored to almost normal in WT mice, whereas leukocyte counts did not recover in S180A animals, pointing to an impaired functionality of hematopoietic stem cells (Fig. 4G). In principle, the observed regenerative defect can be explained by a higher sensitivity of S180A stem cells to 5FU which would lead to a reduction in the LT-HSC pool and failure in reconstitution of the progenitor population after treatment. In support of this hypothesis, 12 days after 5FU injection activation of stem cells led to an increase of the total LSK population in WT animals, but not in S180A mice (Fig. 4H). Concomitantly, the number of LT-HSCs was strongly reduced in S180A animals relative to WT (Fig. 4H, Supplementary Fig. S6B).

Inspired by the hematopoietic stem cell phenotype, we also assessed the regenerative capacity of tissue-specific stem cells in the muscle. By direct intramuscular injection of $BaCl_2$, we induced muscle injury which is subsequently repaired by activation of satellite stem cells. Tissue samples obtained at different time-points after $BaCl_2$ application showed a substantially larger necrotic area 4 days after injection and a delayed recovery of muscle tissue after 12 days in S180A compared to WT mice (Supplementary Fig. S7).

These experimental data indicate that loss of p53 S180 phosphorylation causes an impairment in tissue regeneration. This phenotype is particularly prominent in the bone marrow, which highlights the importance of phosphorylation-mediated inhibition of p53 activity for preservation of hematopoietic stem cell function.

S180A mice show reduced longevity

To better understand the impact of the S180A mutation in the context of the complete organism, we performed deep phenotype analysis on large cohorts of homozygous S180A knock-in and WT littermates (Supplementary Table S3). Pre- and postnatal development of homozygous animals did not differ from wild-type littermates, and by the age of 7-20 weeks they had similar bodyweight, no dysmorphology and no significant alterations in the structure of inner organs (Supplementary Table S3,4). Also, physiological parameters such as cardiovascular and muscle function, energy metabolism, body temperature, behavior and perception were unaffected in homozygous S180A mice (Supplementary Table S4). Clinical chemistry analysis of blood did not show substantial differences between young adult S180A and WT animals (Supplementary Table S2). Detailed hematological and immunological examinations revealed a slight decrease in lymphocytes and increase in granulocyte populations in knock-in females, whereas in males this tendency did not reach

statistical significance (Supplementary Table S2). Thus, we did not detect any major structural or physiological differences in S180A mice, indicating that in normal conditions S180 phosphorylation has only minute effects at most on p53's functions *in vivo*.

However, it is well established that maintenance of different stem cell compartments is critical for longevity and that elevated p53 activity in mice can compromise stem cell function resulting in aging (44-47). When aging cohorts of mice, we noticed that the median overall survival of homozygous S180A was significantly shorter than that of wild-type mice – 568 versus 709 days, respectively (Fig. 5A). Interestingly, several parameters known as markers of aging in mice, such as body weight, lordokyphosis (spinal curvature) and dermal thickness, did not show significant differences (Supplementary Fig. S8). Instead, premature death of S180A mice was accompanied by a general loss of fitness and non-specific systemic diseases such as age-related cardiac and respiratory failure also seen in older WT animals, but not linked to a particular pathology (Table 1). We conclude that in the absence of exogenous genotoxic stress S180A mice have a largely normal phenotype, but show a markedly reduced lifespan resulting from non-specific, age-related systemic diseases.

Loss of S180 phosphorylation enhances tumor suppression

A reduction in DNA-binding cooperativity compromises p53's tumor suppressive function (15,16), prompting us to hypothesize that the increased cooperativity of S180A potentiates tumor suppression. Indeed, we observed a reduction in neoplastic diseases in aged S180A mice (32.3% in WT versus 18.6% in S180A mice, Table 1). To exclude that the tumor incidence is simply reduced because of the shortened lifespan, we explored resistance to experimentally-enforced, oncogene-driven

tumorigenesis using genetically-engineered mouse models of malignant lymphoma and lung cancer.

In the Eμ-*Myc* lymphoma model, enforced overexpression of a *Myc* transgene induces B-cell lymphoma with 100% penetrance (23), and the latency of disease is strongly dependent on p53 status (48). Eμ-*Myc* transgenic mice with a single S180A allele demonstrated a superior median lifespan in comparison to $p53^{+/+}$ littermates (103 versus 91 days, $p<0.0277$) (Fig. 5B). The proportion of long-lived mice, who remained tumor-free longer than 150 days, was more than 2.5 fold higher in the S180A cohort than in the WT group (Fig. 5C). More than 25% of S180A mice, compared to only 10% of WT animals, remained lymphoma-free at this time point (Fig. 5C). Hence, Myc-induced lymphomagenesis was substantially delayed in the absence of S180 phosphorylation.

To assess if loss of S180 phosphorylation also augments p53-mediated tumor suppression in solid tumors, we used a mouse model for Anaplastic Lymphoma Kinase (*ALK*)-positive non-small cell lung cancer (NSCLC), in which prognosis is strongly affected by p53 status (24,49,50). When inducing an *Eml4-Alk* fusion oncogene by intra-tracheal adenoviral delivery of CRISPR/Cas9 nucleases (24), S180A mice displayed pronounced resistance to *Eml4-Alk*-driven tumorigenesis (Fig. 5D). Using sensitive monitoring by bioluminescence imaging (BLI), 7 out of 12 (58%) S180A mice were still tumor-free, when 14 of 16 (88%) WT mice already presented tumors (Fig. 5E). When the animals were analyzed histologically at the experimental endpoint, the overall tumor burden was significantly reduced in S180A mice and 46% of S180A samples were completely tumor-free and displayed only small hyperplastic foci (Fig. 5F,G). The levels of phospho-ERK as a marker for Eml4-Alk activity and the proliferation marker Ki-67 in tumors from S180A and WT mice were similar (Supplementary Fig. S9), suggesting that loss of S180 phosphorylation potentiated the

tumor suppressive function of p53 at early stages of tumorigenesis, but did not change the tumor phenotype – possibly because p53 functions become blunted in established tumors. In conclusion, two independent mouse models of oncogene-driven hematopoietic and lung cancer indicate that loss of S180 phosphorylation can enhance tumor suppression by p53.

Human S183/S185 phosphorylation-deficiency enhances p53-mediated tumor cell apoptosis

To estimate whether phosphorylation-dependent regulation of cooperativity is also relevant for tumor suppressive p53 functions in human cancer cells, we expressed various phospho-mimic and phospho-deficient S183/S185 variants in p53-deficient Saos-2 cells (Fig. 6A,B). While all variants were mounting a cell cycle arrest to similar extent as WT, phospho-mimic variants were impaired in triggering apoptosis – similar to various low-cooperativity variants with mutations of the H1 helix salt bridge residues E180 and R181 (13,39).

To analyze apoptotic functions of the phospho-variants in a more physiological setting, we introduced the phospho-deficient S183A/S185A (AA) and phospho-mimic S183D/S185D (DD) point mutations into HCT116 *TP53*$^{+/-}$ colon cancer cells by CRISPR/Cas9-mediated genome editing. Correct *TP53* gene editing was confirmed by sequencing of exon 5 and full-length p53 cDNA (Fig. 6C). Similar to WT, the AA and DD variants displayed normal nuclear localization and stabilization after treatment with the Mdm2 inhibitor Nutlin-3a or upon genotoxic stress (Fig. 6D,E). Multiple independent clones of HCT116-AA cells showed enhanced DNA damage-induced target gene expression, whereas HCT116-DD clones were transcriptionally compromised compared to HCT116$^{+/-}$. Furthermore, compared to both WT and HCT116-DD cells, HCT116-AA clones demonstrated superior induction of apoptosis

in response to doxorubicin (Fig. 6E,F). Taken together, our results indicate that $p53^{S183/S185}$ phosphorylation limits the tumor suppressive, pro-apoptotic p53 activity in human cancer cells, strongly suggesting that targeting this phosphorylation could synergize with p53-activating drugs and improve cancer therapy responses.

Discussion

p53 suppresses tumorigenesis primarily as a transcription factor that binds DNA cooperatively as a tetramer. Cooperative DNA binding is supported not only by the dedicated oligomerization domain but also by interactions mediated by the DNA binding core domains – in particular via salt-bridges between the H1 helix residues E180 and R181 (17-20). These salt-bridges are indispensable for tumor suppression as proven by the increased cancer susceptibility of E180/R181 mutant knock-in mice and an estimated world-wide number of 34,000 cancer patients per year with salt-bridge mutations (15,16,21). Whether and how p53 DNA binding cooperativity is regulated, however, remained elusive.

Here, we provide evidence that DNA binding cooperativity is influenced by serine residues (S183 and S185 in human p53 and S180 in mouse p53) in direct proximity to the salt-bridge. While post-translational modifications of p53 typically cluster in the intrinsically unstructured N- and C-terminal regions of the protein and are only rarely observed in the DNA binding core domain, several independent mass spectrometry studies have provided evidence for S183/S185 phosphorylation (5-8). As phosphorylation sets a negative charge, we hypothesize that the altered surface charge distribution pattern affects the core domain interactions that are critical for DNA binding cooperativity. Supporting this assumption, it has been recently demonstrated for Raf Kinase Inhibitory Protein (RKIP) that phosphoserine in the vicinity of an intermolecular lysine-glutamate salt bridge competes for the lysine, initiating a partial unfolding event that leads to the dissociation of the salt bridge (38). In addition, it is interesting to note that many S183/S185 phosphorylated peptides identified by mass spectrometry are also R181 methylated (7,8). Given substantial evidence for inter-dependent post-translational protein modification by protein arginine methyltransferases (PRMTs) and kinases (including Aurora B) (51-53), it is tempting

to speculate that sequential or concurrent methylation of R181 reinforces disruption of the E180-R181 salt bridge.

Using multiple phospho-mimetic (S-to-D or S-to-E) p53 variants show a marked reduction in DNA binding and transactivation which is evident most clearly at response elements that deviate from the consensus motif (Fig. 1G,H). The resulting restriction of the target gene spectrum to the most consensus-like response elements translates into a reduced induction of apoptosis (Fig. 6), that is highly characteristic also for cooperativity mutations affecting E180 and R181 (13,14,39), further supporting the idea that S183/S185 phosphorylation reduces DNA binding cooperativity. Of note, while S183 phosphorylation has been linked previously to accelerated p53 degradation through the polyubiquitination–proteasome pathway (5), we did not observe reduced expression levels for phospho-mimic variants despite pronounced changes in p53 activity (Fig. 6B,D, Supplementary Fig. S1D).

Phosphorylation-deficient S-to-A variants displayed a strongly tissue and context-dependent phenotype. Possibly due to an absence of phosphorylation in recombinant p53, phosphorylation-deficient S-to-A variants did not show increased DNA binding *in vitro* (Fig. 1, Supplementary Fig. S1). When expressed from the endogenous *Trp53* gene locus, the mouse S180A variant activated classical p53 target genes in irradiated MEFs (Fig. 3B) and induced apoptosis in irradiated lymphocytes similar to wild-type (Fig. 3C,D). Moreover, when S180A mice were X-irradiated, the degree and extent of IR-induced apoptosis was not increased (Fig. 4C, Supplementary Fig. S3D, S4B) and tissues, in which IR does not induce apoptosis, remained radioresistant (Supplementary Fig. S5). However, pronounced differences were observed in response to chronic stress and with regard to proliferation. The oxidative stress-dependent senescence of primary MEF cultures was accelerated and enhanced in the S180A genotype (Fig. 3F,G) and proliferation in the thymus, spleen and bone marrow

failed to resume properly after DNA damage (Fig. 4D, Supplementary Fig, S3E) resulting in defective recovery from neutropenia (Fig. 4G,H). Overall, this fairly selective hematopoietic phenotype is likely reflecting the exceptional vulnerability of bone marrow stem cells to elevated p53 activity that is also responsible for the bone marrow toxicity observed in patients treated with Mdm2 inhibitors and in mice with deregulated p53 activity (46,54-58). Importantly, this phenotype suggests that S180 phosphorylation has a critical role in dampening DNA damage-triggered p53 activity to preserve the hematopoietic stem cell compartment.

Although young S180A mice did not display any significant differences to wild-type animals (Supplementary Tables S2-4), we observed a marked reduction in lifespan (Fig. 5A). This is reminiscent of early aging phenotypes reported for several mouse models with elevated p53 activity (44-47). However, aging is not a default phenotype resulting from elevated organismal p53 activity as demonstrated by multiple mouse models with enhanced p53-mediated tumor suppression in the absence of premature aging (57,59). Interestingly, $p53^{TSD/-}$ mice with the T21D/S23D mutation, that mimics constitutive phosphorylation of the p53 N-terminus, die by 6 weeks of age exhibiting accelerated aging, which is rescued by deletion of the pro-apoptotic p53 target gene *Bbc3*/*Puma* (46). In striking contrast to this aging-promoting effect of N-terminal phosphorylation, DBD phosphorylation at S180 counteracts premature aging and therefore represents the first post-translational modification of p53 that increases longevity.

Different from mice with aberrant expression of N-terminally truncated p53 (44), the aging phenotype in S180A mice appeared as a more subtle predisposition to premature death by cardiac or respiratory failure without gross alterations in body weight, dermal thickness or osteoporosis-associated lordokyphosis (Table 1, Supplementary Fig. S8). A possible explanation is the rather selective increase of p53

activity in the hematopoietic compartment of S180A mice (Fig. 4). It can be envisioned that the exceptional vulnerability of hematopoietic stem cells to everyday genotoxic insults progressively depletes the hematopoietic stem cell pool and, as p53 activity is controlling clonal competition in the bone marrow (60), eventually decreases the clonal complexity in the bone marrow. Of note, the most extreme form of a reduced HSC clonal complexity, clonal hematopoiesis of indeterminate potential (CHIP) in the elderly, results in an increased risk of all-cause and cardiovascular mortality likely via its effects on immune function (61). We therefore speculate that the loss of hematopoietic stem cell function indirectly compromises other tissues thereby predisposing to a broad range of age-related disorders that reduce the lifespan.

Similar as in other mouse models with elevated p53 activity (44,59), we also observed improved resistance to spontaneous (Table 1) and oncogene-enforced tumorigenesis (Fig. 5). In established tumor cell lines, enforced expression of non-phosphorylatable S183/S185 variants triggered apoptosis more effectively than wild-type p53 and CRISPR-engineered S183/S185-to-A mutations of the endogenous *TP53* gene locus sensitized to chemotherapy-induced apoptosis (Fig. 6). *Vice versa*, phospho-mimic S183/185 mutations reduced p53-mediated apoptosis suggesting that such mutations would be tumorigenic. However, single-nucleotide substitutions cannot change these serine codons (TCA or AGC) to Asp or Glu (GAN), providing an explanation why S183/S185 missense mutations are underrepresented in cancer patients and phospho-mimic mutations at these codons have not been described (Fig. 1B). Together these results reinforce the notion that S183/S185 phosphorylation is not only promoting tumorigenesis but also required for tumor maintenance. Importantly, this suggests inhibition of S183/S185 phosphorylation as a new potential treatment strategy to enhance the pro-apoptotic function of p53 for tumor therapy. Although the role of S183/S185 phosphorylation has not been studied in the context of mutant p53,

it is tempting to speculate that targeting this phosphorylation might not only boost wild-type p53 activity but also rescue some p53 mutants. This might apply in particular to non-hotspot mutants, many of which retain a residual level of DNA binding activity, that might be increased to wild-type levels through improved cooperativity.

Unfortunately, the S183/S185 kinases remain poorly characterized. S183 (mouse S180) is a predicted consensus site for Aurora kinases . Aurora A is known to reduce p53 activity by phosphorylating multiple sites different from S183/S185 (62-64). Aurora B has also been reported to phosphorylate p53 at several sites, including S183 (5,6). Moreover, Aurora A and B were both identified as kinases essential for pluripotency in embryonic stem cells (65). Furthermore, analysis of the TCGA PanCancer Atlas reveals a mutual exclusivity of inactivating *AURKB* alterations (deep deletions and missense mutations) with wild-type p53 status (Supplementary Fig. S10), suggesting that Aurora B might be required for attenuating wild-typ53 function in tumors. Although mass spectrometry has provided evidence for S185 along with S183 phosphorylation (7,8), a S185 kinase has not yet been reported. To exploit the therapeutic potential of boosting the apoptotic activity of p53, it will therefore be of utmost importance to systematically identify the kinases responsible for S183/S185 phosphorylation in tumor cells.

In summary, our study provides evidence at the biochemical, cellular and organismal level that p53 functions in tumorigenesis and aging are balanced at the level of DNA binding cooperativity by serine phosphorylation.

Authors' Contributions

Conceptualization: OT and TS; Molecular biology experiments: OT, LK, CN, AT, JS, MK, SE, MZ, CO; Biochemistry experiments: CO, VD; Animal experiments: SE, GMCC, MHA; Bioinformatics: MM; Genomics: AN; Writing – Original Draft: OT, VD, MHA, TS; Writing – Review and Editing: all.

Acknowledgments

Authors thank Sigrid Bischofsberger, Antje Grzeschiczek, Angela Mühling, Björn Geissert, Franziska Wojciech, Saumya Manmadhan and employees of the animal facility of Marburg University for technical support. We acknowledge support by the Medical Core Facilities (Genomics, Flow Cytometry, X-ray, Small Animal Imaging: 7T-MRI and PET-CT). This work was supported by grants from Deutsche Krebshilfe (111250, 70112623 to TS and 111444 to OT), Deutsche José Carreras Leukämie Stiftung e.V. (09 R/2018 to OT and TS), Deutsche Forschungsgemeinschaft (TRR81 A10 to TS, TI 1028/2-1 to OT, STI 182/13-1 to TS, DO 545/18-1 to VD), German Center for Lung Research (DZL) to TS, BMBF (01KX1012 to MHA, 031L0063 to TS), von Behring-Röntgen Stiftung (65-0004 and 66-LV06 to TS).

References

1. Liu Y, Tavana O, Gu W. p53 modifications: exquisite decorations of the powerful guardian. J Mol Cell Biol **2019**;11:564-77
2. Sykes SM, Mellert HS, Holbert MA, Li K, Marmorstein R, Lane WS*, et al.* Acetylation of the p53 DNA-binding domain regulates apoptosis induction. Mol Cell **2006**;24:841-51
3. Tang Y, Luo J, Zhang W, Gu W. Tip60-dependent acetylation of p53 modulates the decision between cell-cycle arrest and apoptosis. Mol Cell **2006**;24:827-39
4. Tang Y, Zhao W, Chen Y, Zhao Y, Gu W. Acetylation is indispensable for p53 activation. Cell **2008**;133:612-26
5. Gully CP, Velazquez-Torres G, Shin JH, Fuentes-Mattei E, Wang E, Carlock C*, et al.* Aurora B kinase phosphorylates and instigates degradation of p53. Proc Natl Acad Sci U S A **2012**;109:E1513-22
6. Wu L, Ma CA, Zhao Y, Jain A. Aurora B interacts with NIR-p53, leading to p53 phosphorylation in its DNA-binding domain and subsequent functional suppression. J Biol Chem **2011**;286:2236-44
7. DeHart CJ, Chahal JS, Flint SJ, Perlman DH. Extensive post-translational modification of active and inactivated forms of endogenous p53. Mol Cell Proteomics **2014**;13:1-17
8. DeHart CJ, Perlman DH, Flint SJ. Impact of the adenoviral E4 Orf3 protein on the activity and posttranslational modification of p53. J Virol **2015**;89:3209-20
9. Riley T, Sontag E, Chen P, Levine A. Transcriptional control of human p53-regulated genes. Nat Rev Mol Cell Biol **2008**;9:402-12
10. Weinberg RL, Veprintsev DB, Fersht AR. Cooperative binding of tetrameric p53 to DNA. J Mol Biol **2004**;341:1145-59
11. Beno I, Rosenthal K, Levitine M, Shaulov L, Haran TE. Sequence-dependent cooperative binding of p53 to DNA targets and its relationship to the structural properties of the DNA targets. Nucleic Acids Res **2011**;39:1919-32
12. Weinberg RL, Veprintsev DB, Bycroft M, Fersht AR. Comparative binding of p53 to its promoter and DNA recognition elements. J Mol Biol **2005**;348:589-96
13. Schlereth K, Beinoraviciute-Kellner R, Zeitlinger MK, Bretz AC, Sauer M, Charles JP*, et al.* DNA binding cooperativity of p53 modulates the decision between cell-cycle arrest and apoptosis. Mol Cell **2010**;38:356-68
14. Schlereth K, Heyl C, Krampitz AM, Mernberger M, Finkernagel F, Scharfe M*, et al.* Characterization of the p53 cistrome--DNA binding cooperativity dissects p53's tumor suppressor functions. PLoS Genet **2013**;9:e1003726
15. Timofeev O, Schlereth K, Wanzel M, Braun A, Nieswandt B, Pagenstecher A*, et al.* p53 DNA binding cooperativity is essential for apoptosis and tumor suppression in vivo. Cell Rep **2013**;3:1512-25
16. Timofeev O, Klimovich B, Schneikert J, Wanzel M, Pavlakis E, Noll J*, et al.* Residual apoptotic activity of a tumorigenic p53 mutant improves cancer therapy responses. EMBO J **2019**;38:e102096
17. Dehner A, Klein C, Hansen S, Muller L, Buchner J, Schwaiger M*, et al.* Cooperative binding of p53 to DNA: regulation by protein-protein interactions through a double salt bridge. Angew Chem Int Ed Engl **2005**;44:5247-51
18. Klein C, Planker E, Diercks T, Kessler H, Kunkele KP, Lang K*, et al.* NMR spectroscopy reveals the solution dimerization interface of p53 core domains bound to their consensus DNA. J Biol Chem **2001**;276:49020-7

19. Kitayner M, Rozenberg H, Kessler N, Rabinovich D, Shaulov L, Haran TE*, et al.* Structural basis of DNA recognition by p53 tetramers. Mol Cell **2006**;22:741-53
20. Kitayner M, Rozenberg H, Rohs R, Suad O, Rabinovich D, Honig B*, et al.* Diversity in DNA recognition by p53 revealed by crystal structures with Hoogsteen base pairs. Nat Struct Mol Biol **2010**;17:423-9
21. Kang JG, Lago CU, Lee JE, Park JH, Donnelly MP, Starost MF*, et al.* A Mouse Homolog of a Human TP53 Germline Mutation Reveals a Lipolytic Activity of p53. Cell Rep **2020**;30:783-92 e5
22. Leroy B, Anderson M, Soussi T. TP53 mutations in human cancer: database reassessment and prospects for the next decade. Hum Mutat **2014**;35:672-88
23. Adams JM, Harris AW, Pinkert CA, Corcoran LM, Alexander WS, Cory S*, et al.* The c-myc oncogene driven by immunoglobulin enhancers induces lymphoid malignancy in transgenic mice. Nature **1985**;318:533-8
24. Maddalo D, Manchado E, Concepcion CP, Bonetti C, Vidigal JA, Han YC*, et al.* In vivo engineering of oncogenic chromosomal rearrangements with the CRISPR/Cas9 system. Nature **2014**;516:423-7
25. DuPage M, Dooley AL, Jacks T. Conditional mouse lung cancer models using adenoviral or lentiviral delivery of Cre recombinase. Nat Protoc **2009**;4:1064-72
26. Sperringer JE, Grange RW. In Vitro Assays to Determine Skeletal Muscle Physiologic Function. Methods Mol Biol **2016**;1460:271-91
27. Hardy D, Besnard A, Latil M, Jouvion G, Briand D, Thepenier C*, et al.* Comparative Study of Injury Models for Studying Muscle Regeneration in Mice. PLoS One **2016**;11:e0147198
28. Gailus-Durner V, Fuchs H, Becker L, Bolle I, Brielmeier M, Calzada-Wack J*, et al.* Introducing the German Mouse Clinic: open access platform for standardized phenotyping. Nat Methods **2005**;2:403-4
29. Fuchs H, Gailus-Durner V, Adler T, Aguilar-Pimentel JA, Becker L, Calzada-Wack J*, et al.* Mouse phenotyping. Methods **2011**;53:120-35
30. Rathkolb B, Hans W, Prehn C, Fuchs H, Gailus-Durner V, Aigner B*, et al.* Clinical Chemistry and Other Laboratory Tests on Mouse Plasma or Serum. Curr Protoc Mouse Biol **2013**;3:69-100
31. Holter SM, Garrett L, Einicke J, Sperling B, Dirscherl P, Zimprich A*, et al.* Assessing Cognition in Mice. Curr Protoc Mouse Biol **2015**;5:331-58
32. Young L, Sung J, Stacey G, Masters JR. Detection of Mycoplasma in cell cultures. Nat Protoc **2010**;5:929-34
33. Matsumura I, Ellington AD. In vitro evolution of thermostable p53 variants. Protein Sci **1999**;8:731-40
34. Nikolova PV, Henckel J, Lane DP, Fersht AR. Semirational design of active tumor suppressor p53 DNA binding domain with enhanced stability. Proc Natl Acad Sci U S A **1998**;95:14675-80
35. Chen C, Gorlatova N, Kelman Z, Herzberg O. Structures of p63 DNA binding domain in complexes with half-site and with spacer-containing full response elements. Proc Natl Acad Sci U S A **2011**;108:6456-61
36. Amend SR, Valkenburg KC, Pienta KJ. Murine Hind Limb Long Bone Dissection and Bone Marrow Isolation. J Vis Exp **2016**
37. Gao J, Aksoy BA, Dogrusoz U, Dresdner G, Gross B, Sumer SO*, et al.* Integrative analysis of complex cancer genomics and clinical profiles using the cBioPortal. Sci Signal **2013**;6:pl1
38. Skinner JJ, Wang S, Lee J, Ong C, Sommese R, Sivaramakrishnan S*, et al.* Conserved salt-bridge competition triggered by phosphorylation regulates the protein interactome. Proc Natl Acad Sci U S A **2017**;114:13453-8

39. Schlereth K, Charles JP, Bretz AC, Stiewe T. Life or death: p53-induced apoptosis requires DNA binding cooperativity. Cell Cycle **2010**;9:4068-76
40. Parrinello S, Samper E, Krtolica A, Goldstein J, Melov S, Campisi J. Oxygen sensitivity severely limits the replicative lifespan of murine fibroblasts. Nat Cell Biol **2003**;5:741-7
41. Huang J, Yang J, Maity B, Mayuzumi D, Fisher RA. Regulator of G protein signaling 6 mediates doxorubicin-induced ATM and p53 activation by a reactive oxygen species-dependent mechanism. Cancer Res **2011**;71:6310-9
42. Demaria M, O'Leary MN, Chang J, Shao L, Liu S, Alimirah F*, et al.* Cellular Senescence Promotes Adverse Effects of Chemotherapy and Cancer Relapse. Cancer Discov **2017**;7:165-76
43. Chambers SM, Shaw CA, Gatza C, Fisk CJ, Donehower LA, Goodell MA. Aging hematopoietic stem cells decline in function and exhibit epigenetic dysregulation. PLoS Biol **2007**;5:e201
44. Tyner SD, Venkatachalam S, Choi J, Jones S, Ghebranious N, Igelmann H*, et al.* p53 mutant mice that display early ageing-associated phenotypes. Nature **2002**;415:45-53
45. Maier B, Gluba W, Bernier B, Turner T, Mohammad K, Guise T*, et al.* Modulation of mammalian life span by the short isoform of p53. Genes Dev **2004**;18:306-19
46. Liu D, Ou L, Clemenson GD, Jr., Chao C, Lutske ME, Zambetti GP*, et al.* Puma is required for p53-induced depletion of adult stem cells. Nat Cell Biol **2010**;12:993-8
47. Zhao Y, Wu L, Yue X, Zhang C, Wang J, Li J*, et al.* A polymorphism in the tumor suppressor p53 affects aging and longevity in mouse models. Elife **2018**;7
48. Eischen CM, Weber JD, Roussel MF, Sherr CJ, Cleveland JL. Disruption of the ARF-Mdm2-p53 tumor suppressor pathway in Myc-induced lymphomagenesis. Genes Dev **1999**;13:2658-69
49. Christopoulos P, Dietz S, Kirchner M, Volckmar AL, Endris V, Neumann O*, et al.* Detection of TP53 Mutations in Tissue or Liquid Rebiopsies at Progression Identifies ALK+ Lung Cancer Patients with Poor Survival. Cancers (Basel) **2019**;11
50. Kron A, Alidousty C, Scheffler M, Merkelbach-Bruse S, Seidel D, Riedel R*, et al.* Impact of TP53 mutation status on systemic treatment outcome in ALK-rearranged non-small-cell lung cancer. Ann Oncol **2018**
51. Hsu JM, Chen CT, Chou CK, Kuo HP, Li LY, Lin CY*, et al.* Crosstalk between Arg 1175 methylation and Tyr 1173 phosphorylation negatively modulates EGFR-mediated ERK activation. Nat Cell Biol **2011**;13:174-81
52. Albrecht LV, Ploper D, Tejeda-Munoz N, De Robertis EM. Arginine methylation is required for canonical Wnt signaling and endolysosomal trafficking. Proc Natl Acad Sci U S A **2018**;115:E5317-E25
53. Kim S, Kim NH, Park JE, Hwang JW, Myung N, Hwang KT*, et al.* PRMT6-mediated H3R2me2a guides Aurora B to chromosome arms for proper chromosome segregation. Nat Commun **2020**;11:612
54. Andreeff M, Kelly KR, Yee K, Assouline S, Strair R, Popplewell L*, et al.* Results of the Phase I Trial of RG7112, a Small-Molecule MDM2 Antagonist in Leukemia. Clin Cancer Res **2016**;22:868-76
55. Abbas HA, Maccio DR, Coskun S, Jackson JG, Hazen AL, Sills TM*, et al.* Mdm2 is required for survival of hematopoietic stem cells/progenitors via dampening of ROS-induced p53 activity. Cell Stem Cell **2010**;7:606-17

56. Ringshausen I, O'Shea CC, Finch AJ, Swigart LB, Evan GI. Mdm2 is critically and continuously required to suppress lethal p53 activity in vivo. Cancer Cell **2006**;10:501-14
57. Mendrysa SM, O'Leary KA, McElwee MK, Michalowski J, Eisenman RN, Powell DA*, et al.* Tumor suppression and normal aging in mice with constitutively high p53 activity. Genes Dev **2006**;20:16-21
58. Terzian T, Wang Y, Van Pelt CS, Box NF, Travis EL, Lozano G. Haploinsufficiency of Mdm2 and Mdm4 in tumorigenesis and development. Mol Cell Biol **2007**;27:5479-85
59. Garcia-Cao I, Garcia-Cao M, Martin-Caballero J, Criado LM, Klatt P, Flores JM*, et al.* "Super p53" mice exhibit enhanced DNA damage response, are tumor resistant and age normally. EMBO J **2002**;21:6225-35
60. Bondar T, Medzhitov R. p53-mediated hematopoietic stem and progenitor cell competition. Cell Stem Cell **2010**;6:309-22
61. Jaiswal S, Ebert BL. Clonal hematopoiesis in human aging and disease. Science **2019**;366
62. Katayama H, Sasai K, Kawai H, Yuan ZM, Bondaruk J, Suzuki F*, et al.* Phosphorylation by aurora kinase A induces Mdm2-mediated destabilization and inhibition of p53. Nat Genet **2004**;36:55-62
63. Liu Q, Kaneko S, Yang L, Feldman RI, Nicosia SV, Chen J*, et al.* Aurora-A abrogation of p53 DNA binding and transactivation activity by phosphorylation of serine 215. J Biol Chem **2004**;279:52175-82
64. Vilgelm AE, Pawlikowski JS, Liu Y, Hawkins OE, Davis TA, Smith J*, et al.* Mdm2 and aurora kinase a inhibitors synergize to block melanoma growth by driving apoptosis and immune clearance of tumor cells. Cancer Res **2015**;75:181-93
65. Lee DF, Su J, Ang YS, Carvajal-Vergara X, Mulero-Navarro S, Pereira CF*, et al.* Regulation of embryonic and induced pluripotency by aurora kinase-p53 signaling. Cell Stem Cell **2012**;11:179-94

§German Mouse Clinic Consortium: Contributing authors

Antonio Aguilar-Pimentel[1]

Carsten Schmidt-Weber[2]

Lore Becker1

Thomas Klopstock[3,9,10,11]

Yi-Li Cho[1]

Dirk H Busch[4]

Nadine Spielmann[1]

Oana Amarie[1]

Raffaele Gerlini[1,7]

Lillian Garrett[1,5]

Sabine M. Hölter[1,5,12]

Wolfgang Wurst[5,9,10,12]

Julia Calzada-Wack[1]

Adrián Sanz-Moreno[1]

Tanja Klein-Rodewald[1]

Birgit Rathkolb[1,6,7]

Eckhard Wolf[6]

Manuela Östereicher[1]

Gregor Miller[1]

Holger Maier[1]

Claudia Stoeger[1]

Stefanie Leuchtenberger[1]

Valérie Gailus-Durner[1]

Helmut Fuchs[1]

[1] German Mouse Clinic, Institute of Experimental Genetics, Helmholtz Zentrum München, German Research Center for Environmental Health GmbH, Ingolstädter Landstrasse 1, 85764 Neuherberg, Germany

[2] Center of Allergy & Environment (ZAUM), Technische Universität München, and Helmholtz Zentrum München, Ingolstädter Landstrasse, 85764 Neuherberg, Germany

[3] Department of Neurology, Friedrich-Baur-Institut, Ludwig-Maximilians-Universität München, Ziemssenstrasse 1a, 80336 Munich, Germany

[4] Institute for Medical Microbiology, Immunology and Hygiene, Technical University of Munich, Trogerstrasse 30, 81675 Munich, Germany

[5] Institute of Developmental Genetics, Helmholtz Zentrum München, German Research Center for Environmental Health GmbH, Ingolstädter Landstrasse 1, 85764 Neuherberg, Germany

[6] Ludwig-Maximilians-Universität München, Gene Center, Institute of Molecular Animal Breeding and Biotechnology, Feodor-Lynen Strasse 25, 81377 Munich, Germany

[7] Member of German Center for Diabetes Research (DZD), Ingolstädter Landstraße 1, 85764 Neuherberg, Germany

[8] Chair of Experimental Genetics, Center of Life and Food Sciences Weihenstephan, Technische Universität München, Ingolstädter Landstrasse 1, 85354 Freising-Weihenstephan, Germany

[9] Deutsches Institut für Neurodegenerative Erkrankungen (DZNE) Site Munich, Schillerstrasse 44, 80336 Munich, Germany

[10] Munich Cluster for Systems Neurology (SyNergy), Adolf-Butenandt-Institut, Ludwig-Maximilians-Universität München, Schillerstrasse 44, 80336 Munich, Germany

[11] German Network for Mitochondrial Disorders (mitoNET)

[12] Technische Universität München-Weihenstephan, Chair of Developmental Genetics, 85764 Neuherberg, Germany

Table 1.

Necropsy results.

Major pathology	+/+		SA/SA	
Neoplasm	10	32.3%	8	18.6%
Nonspecific systemic disease*	15	48.4%	26	60.5%
Ocular lesion**	3	9.7%	3	7.0%
Other***	1	3.2%	4	9.3%
Unknown	2	6.5%	2	4.7%
Total number of examined animals	31	100%	43	100%

*Nonspecific systemic disease: age-related or -induced lesions including cardiac and respiratory failure; sepsis and DIC; female reproductive diseases or male urogenital diseases, etc.

** Ocular lesion: includes corneal ulceration and chronic keratitis

*** Others: include rectal prolapse, gastrointestinal bleedings, megaesophagus, nephropathy.

Figure 1.

S183/S185 variants are underrepresented in cancer and affect DNA binding and transcriptional activity. **A,** Evolutionary conservation of serine residues in proximity to helix H1 (aa 176-181). **B,** Spectrum of *TP53* mutations in cancer patients (UMD database). **C-D,** Thermal Shift Assay of purified, thermostable $p53^{TS}$(41-356) variants. **C,** Representative melting curves. Normalized first deviation of the fluorescence intensity is plotted against the temperature. Peak maxima reflect the apparent melting temperature of the protein. **D,** Melting temperatures extracted from melting curves recorded in triplicates. Shown are single data points and mean ± standard deviation (SD). **E-F,** Surface Plasmon Resonance (SPR) affinity curves of $p53^{TS}$(41-356) variants binding to the p21 response element. The 20 bp core sequence of the p21 RE was immobilized onto a streptavidin (SA) coated chip and a random DNA sequence was used for the reference cell to subtract unspecific DNA binding. Data points were extracted by equilibrium analysis of sensograms and normalized. Plotted triplicates were globally fitted with a non-linear, least squares regression using a single-exponential one-site binding model. p53 monomer concentration is shown as $\log_{10}$ to resolve all binding curves. **F,** Affinities of $p53^{TS}$(41-356) variants to the p21 RE. Shown are mean K_D and 95% confidence interval. The K_D of p53 R273H could not be determined as saturation was not reached. **G,** Electrophoretic Mobility Shift Assays (EMSA) of *in vitro* translated full-length p53 proteins and oligonucleotides containing denoted p53 response elements (REs). Shown is the intensity of p53 variant DNA-complexes normalized to wild-type p53 (WT) as single data points and mean ± SD (n=2). **F,** Luciferase reporter assays. H1299 cells were co-transfected with the indicated p53 variants and luciferase reporter vectors containing different p53 REs. EV, empty vector. Results were normalized to WT and are shown as single data points and mean ± SD (n=3).

Figure 2.

S180A mutation increases DNA binding and transcriptional activity. **A-D**, p53 ChIP-seq analysis of MEFs ±10 μM Nutlin-3a for 16 hours. **A**, All p53 binding peaks called in Nutlin-treated wild-type and $p53^{S180A}$ MEFs were merged. Hyper-chipable regions also called in p53-/- MEFs were removed, yielding a total of 622 p53 binding peaks, which were sorted from top to bottom by the normalized ChIP-seq signal in Nutlin-treated p53 wild-type cells. Shown are normalized signal intensities for 2 kb regions surrounding the peak summit. **B**, Motif logo for the best motif discovered with MEME-ChIP in the top 50% of p53 binding sites shown in (**A**). **C**, Average signal intensity plots (averaged read count over all genomic regions normalized to the maximum signal) of all binding peaks centered on the peak summit. **D**, Co-occurrence of different dinucleotides at the center of the two p53 RE half sites, i.e. the WW positions 5, 6 and 15,16 in the p53RE consensus motif RRRCWWGYYY.RRRCWWGYYY). AA and TT were considered equivalent. Shown are base frequencies at the indicated positions for the top and bottom 10% of p53 binding sites shown in (**A**). **E-H**, RNA-seq analysis of untreated and Nutlin-3a treated low-passage MEFs (n=3 independent MEF preparations per genotype). **E-F**, Gene set enrichment analysis (GSEA). **E**, GSEA plot for the MSigDB HALLMARK p53 pathway gene set. **F**, Summary of GSEA results for different p53-related gene sets. NES, normalized enrichment score; nom p, nominal p-value. **G**, Heatmap of p53-activated target genes, i.e. all expressed protein-coding genes, which have a p53 ChIP-seq peak and are activated by Nutlin-3a (FC≥1.5) in WT or S180A cells. Shown are z-transformed RNA expression values. Target genes were sorted from top to bottom by the intensity (log10 FPM, fragments per million) of the p53 WT ChIP-seq peak (*left*). Genes included in p53-related gene sets are labelled in black (*right*). **H**, Expression of the n=37 top and 38 bottom p53-activated target genes from (**G**) in Nutlin-3a treated WT or S180A MEFs. Shown is the mean ± SEM

(two-tailed Mann Whitney test); RPKM, reads per kilobase of exon per million reads mapped.

Figure 3.

S180A reduces proliferative potential and enhances senescence. **A-B**, Early passage $p53^{+/+}$ (+/+) and homozygous S180A (SA/SA) MEFs were irradiated with 6 Gy. **A**, Western blot. **B**, Quantitative RT-PCR for indicated p53 target genes. Shown is expression normalized to β-actin as mean ± SD (n=5 batches of MEFs per genotype). **C-D**, Primary thymocytes or splenocytes were irradiated *ex vivo*. Shown is specific survival as mean ± SD (n=3 per genotype for each dose and time-point). **E**, Proliferative potential of MEFs with indicated genotypes cultured at ambient (21%) or physiological (3%) oxygen level. Shown are cumulative population doublings. **F-G**, Low-passage primary MEFs from littermates (n=3 per genotype, n=6 replicates each) were treated at low passage with low dose doxorubicin (50 ng/ml) for 48 h and stained for senescence-associated β-galactosidase (SA-β-gal). **F**, Representative images. **G**, Percentage of SA-β-gal positive cells. Shown are single data points and mean ± SD (unpaired, two-sided t-test).

Figure 4.

Delayed recovery of hematopoietic compartment from DNA damage in S180A mice. **A-E**, Whole-body irradiation (6 Gy) of $p53^{+/+}$ (+/+) and homozygous S180A (SA/SA) mice. Immunohistochemistry of bone marrow for (**A**) p53-pSer15, (**B**) p21/Cdkn1a, (**C**) apoptosis/TUNEL, (**D**) proliferation/BrdU. **E**, Shown is the number of BrdU-positive cells 72 h after IR in 500×500 μm^2 fields of view. Two-sided Mann-Whitney test (n=3 mice per genotype with 2-4 samples per mouse). **F**, Flow cytometry analysis of bone marrow from femurs of untreated mice after removal of erythrocytes. Left: total cellularity of SA/SA samples (n=10) normalized to the mean of +/+ samples (n=12). Middle and right: fraction of $Lin^{-/low}$, $Sca1^{+}$, $c\text{-}kit^{+}$ (LSK) and LSK, $CD34^{-}$, $Flk2^{-}$ cells (n=6 per genotype). Two-sided Mann-Whitney test. The gating strategy is shown in Supplementary Fig. S5. **G**, Total leukocyte concentration of peripheral blood collected at indicated time-points before and after 5FU treatment of mice. Multiple two-sided t-tests in combination with the False Discovery Rate approach. Reported are FDR q-values (n=9 per time-point and genotype). **H**, Flow cytometry analysis of bone marrow samples 12 days after 5FU treatment as described in (**F**). Two-sided Mann-Whitney test (n=12 for +/+, n=10 for SA/SA). All graphs show individual data points and mean ± SD.

Figure 5.

Reduced lifespan and enhanced tumor suppression in S180A mice. **A**, Kaplan-Meier plots for overall survival (logrank test). **B-C**, *Myc*-driven B-cell lymphoma in $p53^{+/+}$ and $p53^{S180A}$ mice. **B**, Kaplan-Meier plots for tumor-free survival (logrank test). **C**, Mortality in different age groups (Chi-square test). **D-G**, *Eml4-Alk*-driven non-small cell lung cancer in $p53^{+/+}$ and $p53^{S180A}$ mice. **D**, Representative lung MRIs of 4 representative mice of each group at indicated time-points after infection with *Eml4-Alk* CRISPR-adenovirus. Arrowheads indicate tumors. **E**, Percentages of tumor-free animals at last bioluminescence imaging before $p53^{+/+}$ controls animals reached the endpoint. **F**, Percentage of tumor area relative to total area per section (Mann-Whitney test, n=13 per genotype). **G**, Representative HE-stained lung sections.

Figure 6.

S183/S185 phosphorylation-deficiency sensitizes human cancer cells to p53-mediated apoptosis. **A-B**, p53-null Saos-2 osteosarcoma cells were infected with adenovirus expressing different $p53^{S183/S185}$ phospho-variants (red, phospho-deficient; blue, phospho-mimic) and wild-type p53 (WT) or GFP as controls. **A**, Representative cell cycle profiles. **B**, Quantification of cell cycle phase distribution by ModFit analysis. Bottom panel: Western blot documenting comparable expression of all p53 variants. **C-E**, HCT116 $p53^{+/-}$ cells were targeted with CRISPR technology to express the S183A.S185A (AA) and S183D.S185D (DD) variants from the endogenous *TP53* gene locus. **C**, cDNA sequencing results (reverse strand) of a representative AA/– and DD/– clone. **D**, Representative p53 immunofluorescence images of indicated cell lines untreated and treated 16 h with 10 μM Nutlin-3a. **E**, Western blot of different independent cell clones untreated and 24 h after treatment with 0.25 μg/ml doxorubicin. HCT116 $p53^{+/-}$ and $p53^{-/-}$ cells are shown as controls. **F**, Quantification of apoptosis by Annexin V flow cytometry. Cell clones of indicated p53 genotypes were treated 24 h with 0.25 μg/ml doxorubicin or left untreated (control). Shown are individual data points and mean ± SD; FDR q-values of multiple two-sided t-tests in combination with the False Discovery Rate approach.

Figure 1

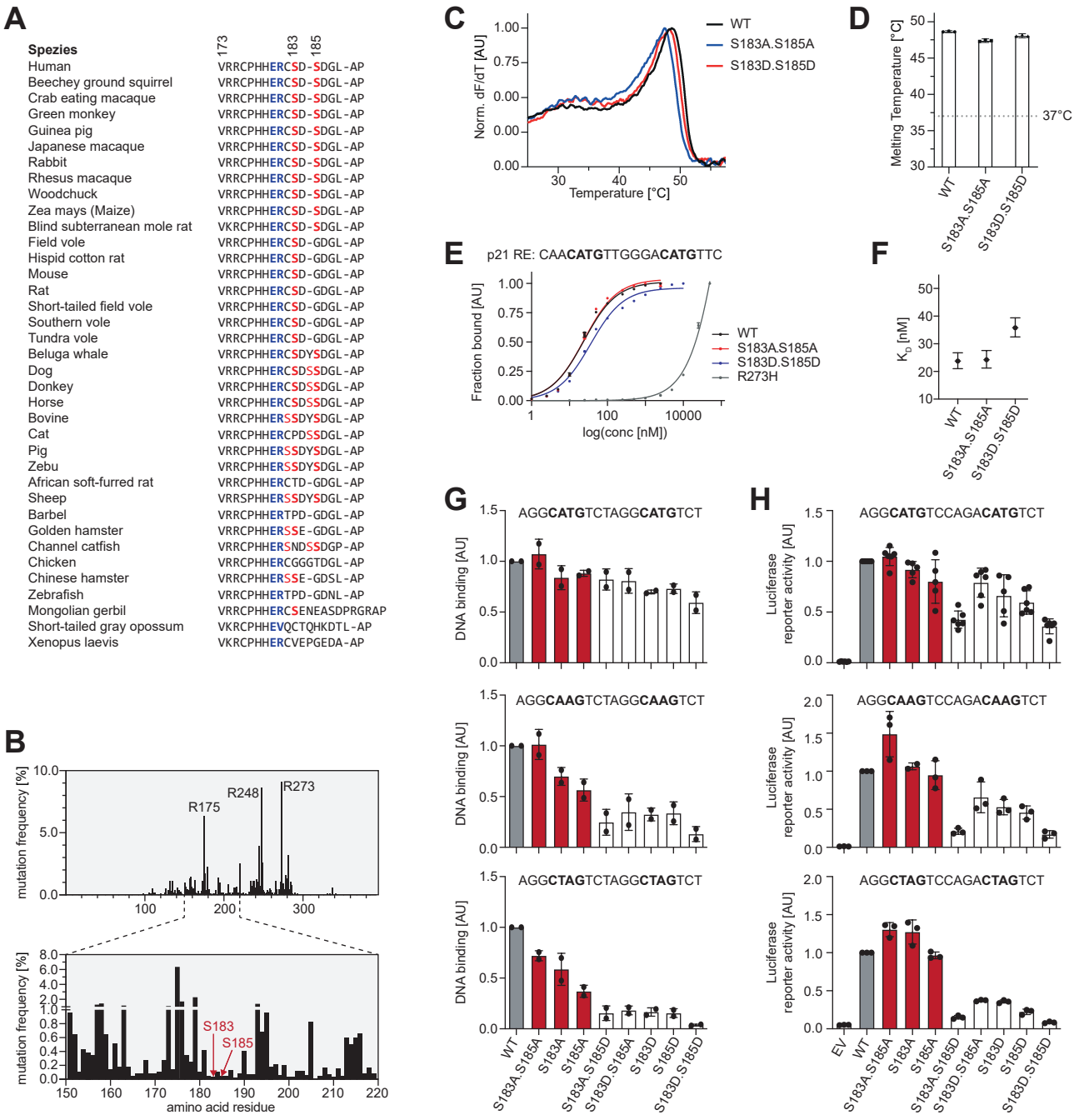

Author Manuscript Published OnlineFirst on September 1, 2020; DOI: 10.1158/0008-5472.CAN-20-2002
Author manuscripts have been peer reviewed and accepted for publication but have not yet been edited.

Figure 2

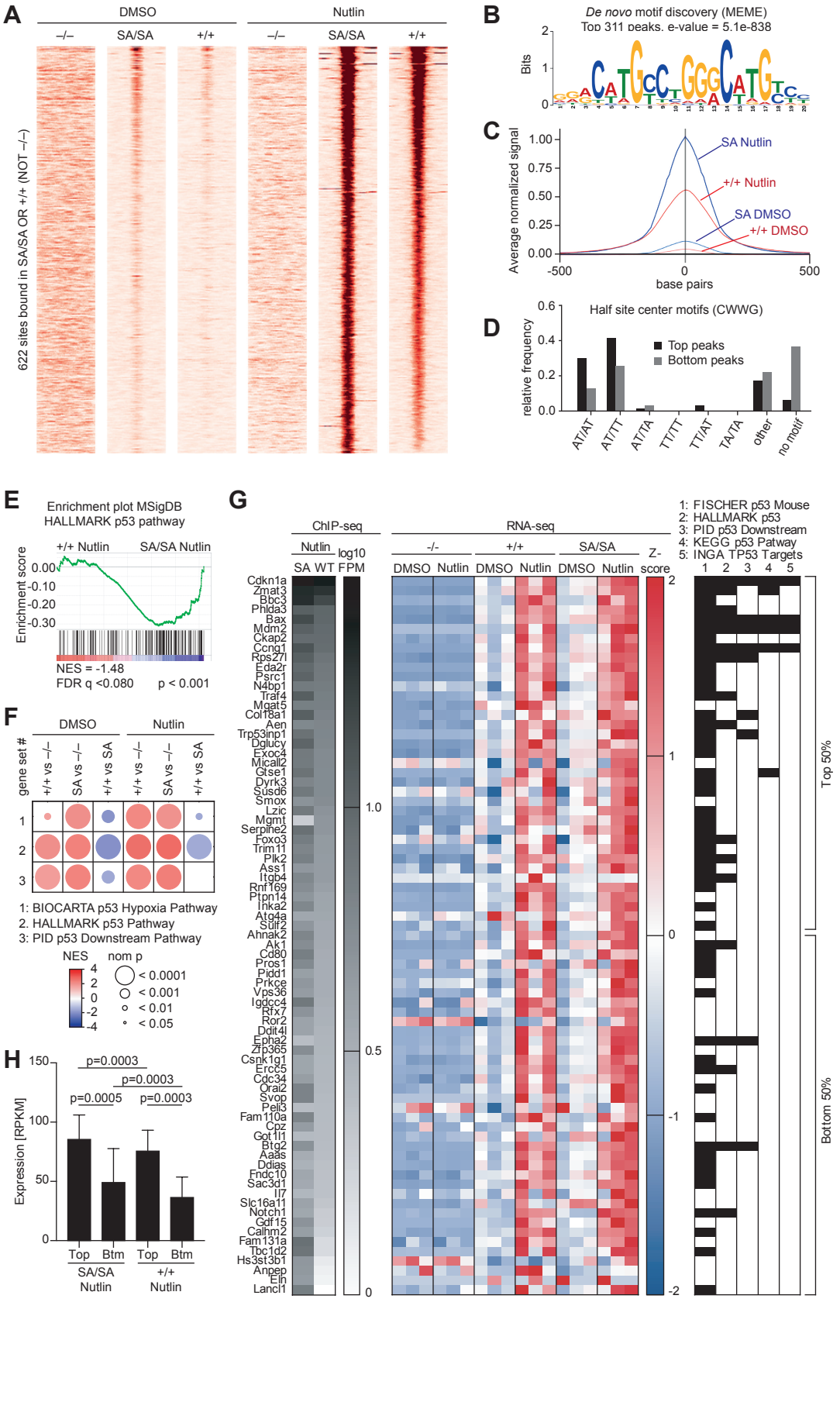

Author Manuscript Published OnlineFirst on September 1, 2020; DOI: 10.1158/0008-5472.CAN-20-2002
Author manuscripts have been peer reviewed and accepted for publication but have not yet been edited.

Figure 3

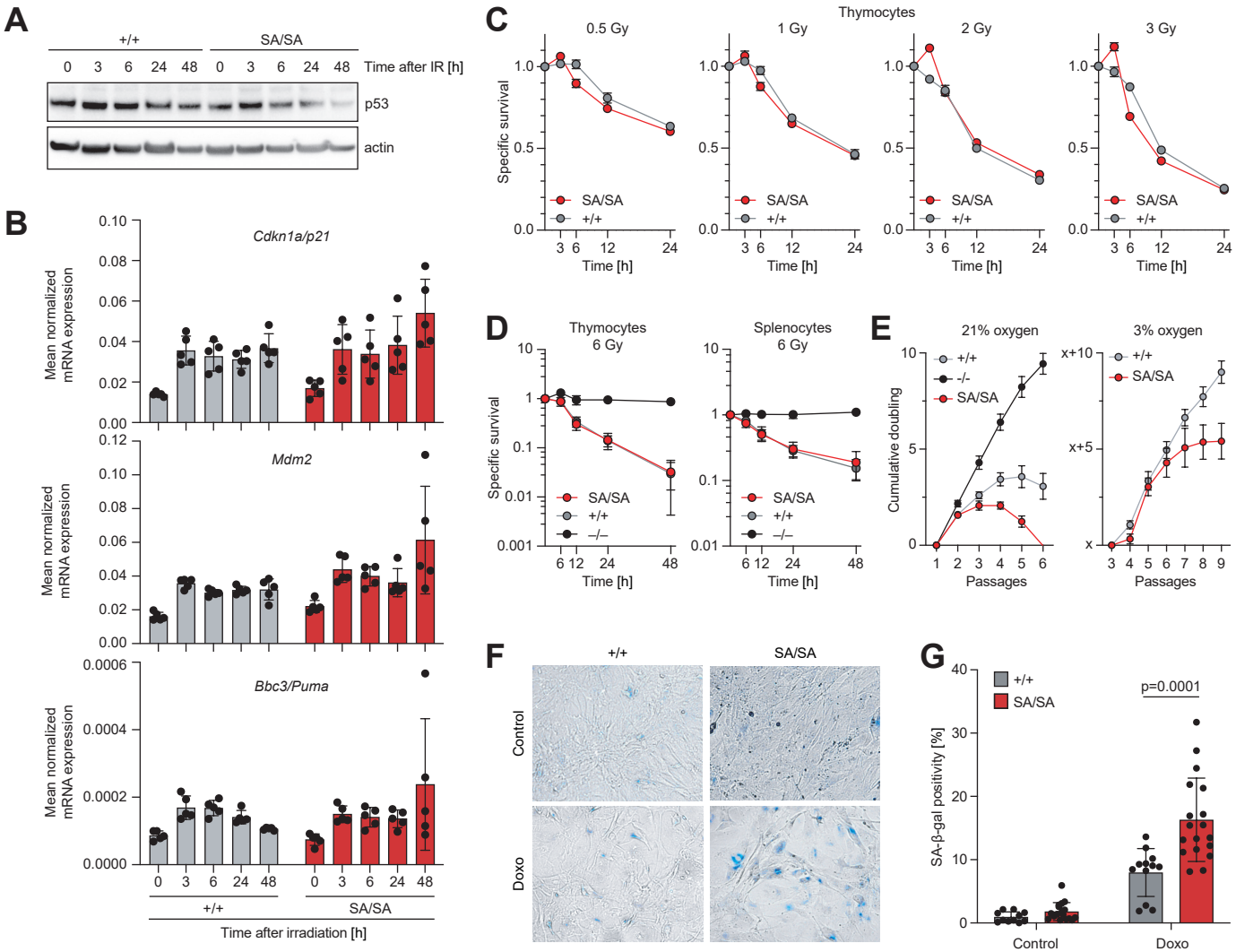

Author Manuscript Published OnlineFirst on September 1, 2020; DOI: 10.1158/0008-5472.CAN-20-2002
Author manuscripts have been peer reviewed and accepted for publication but have not yet been edited.

Figure 4

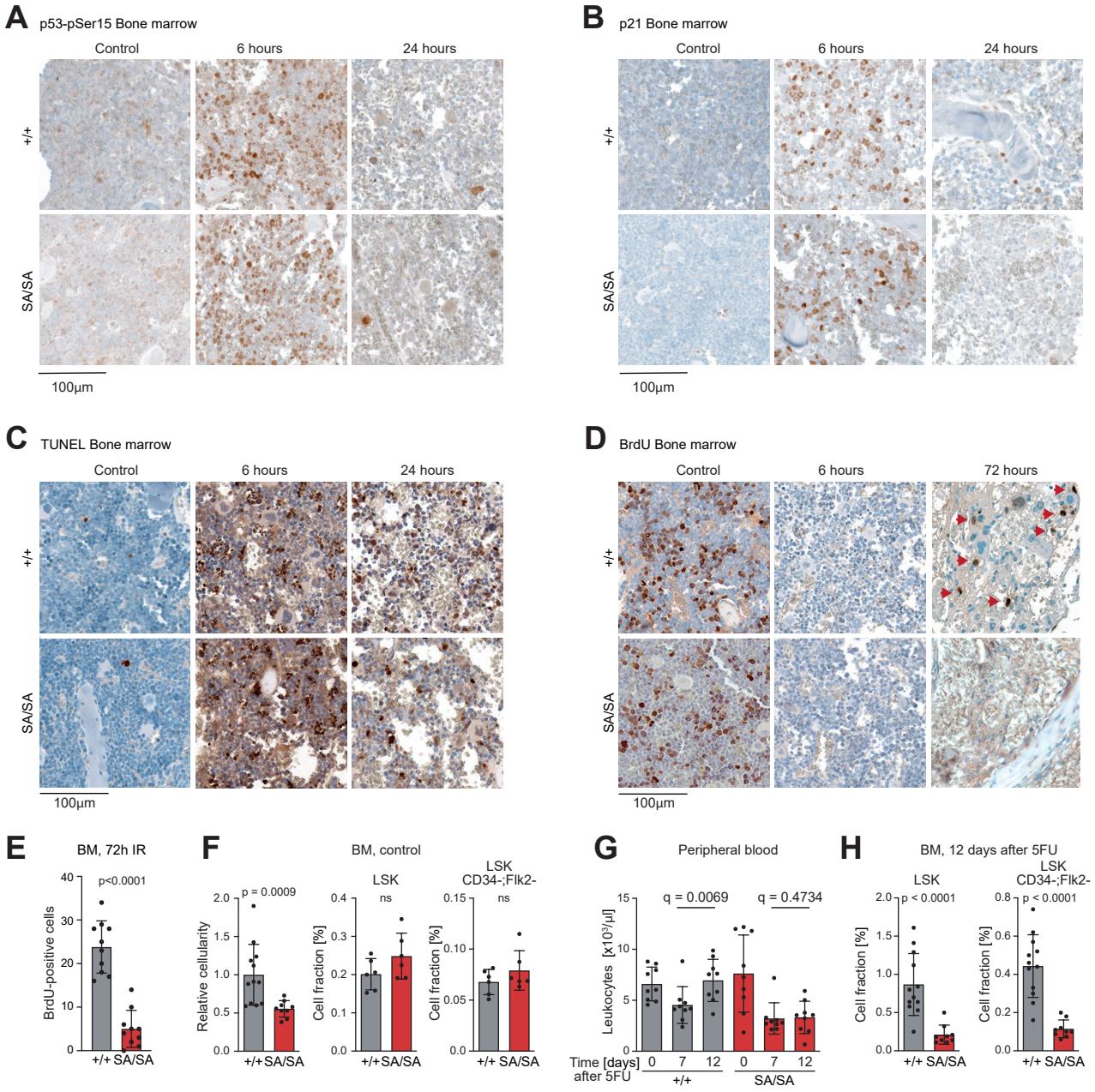

Author Manuscript Published OnlineFirst on September 1, 2020; DOI: 10.1158/0008-5472.CAN-20-2002
Author manuscripts have been peer reviewed and accepted for publication but have not yet been edited.

Figure 5

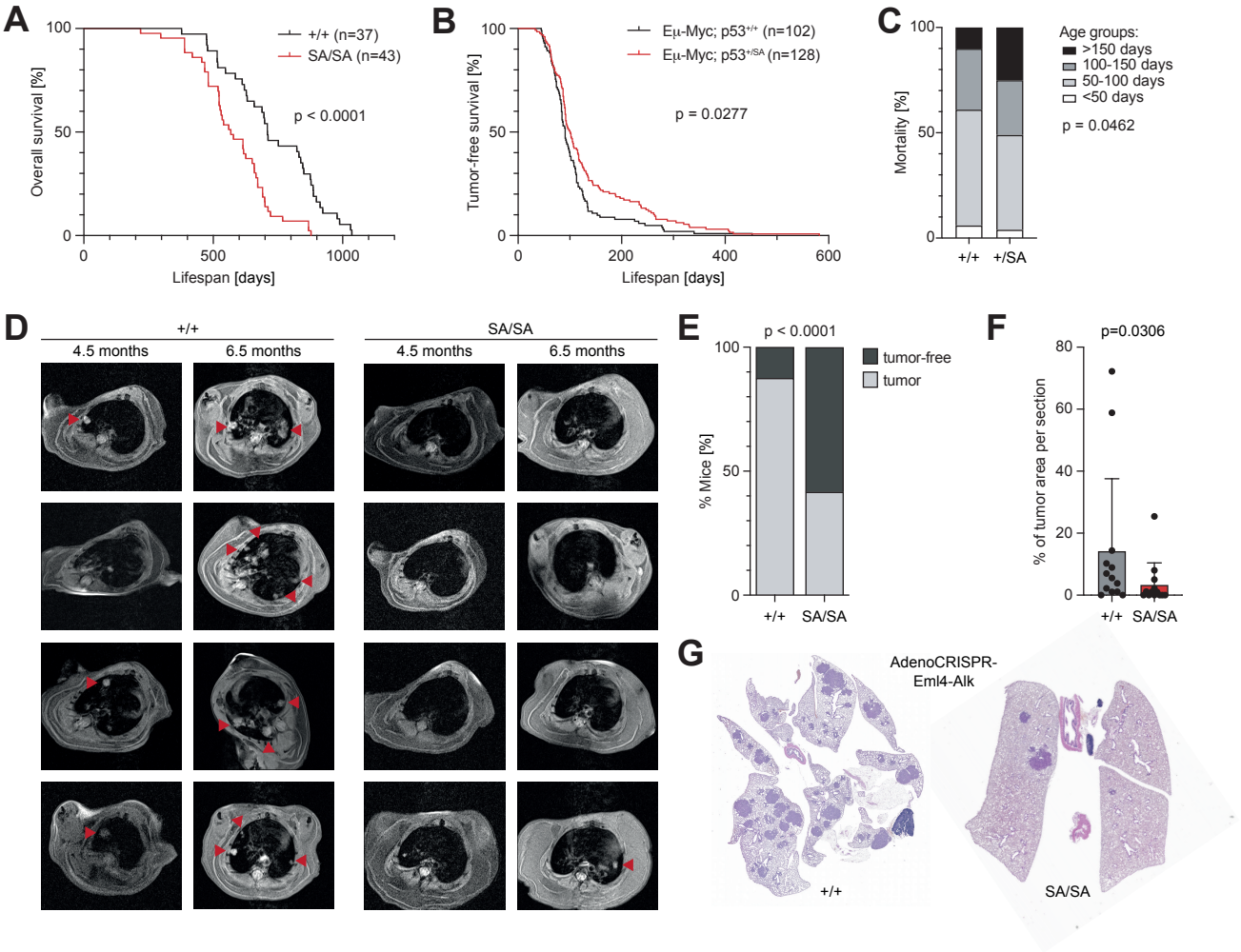

Figure 6

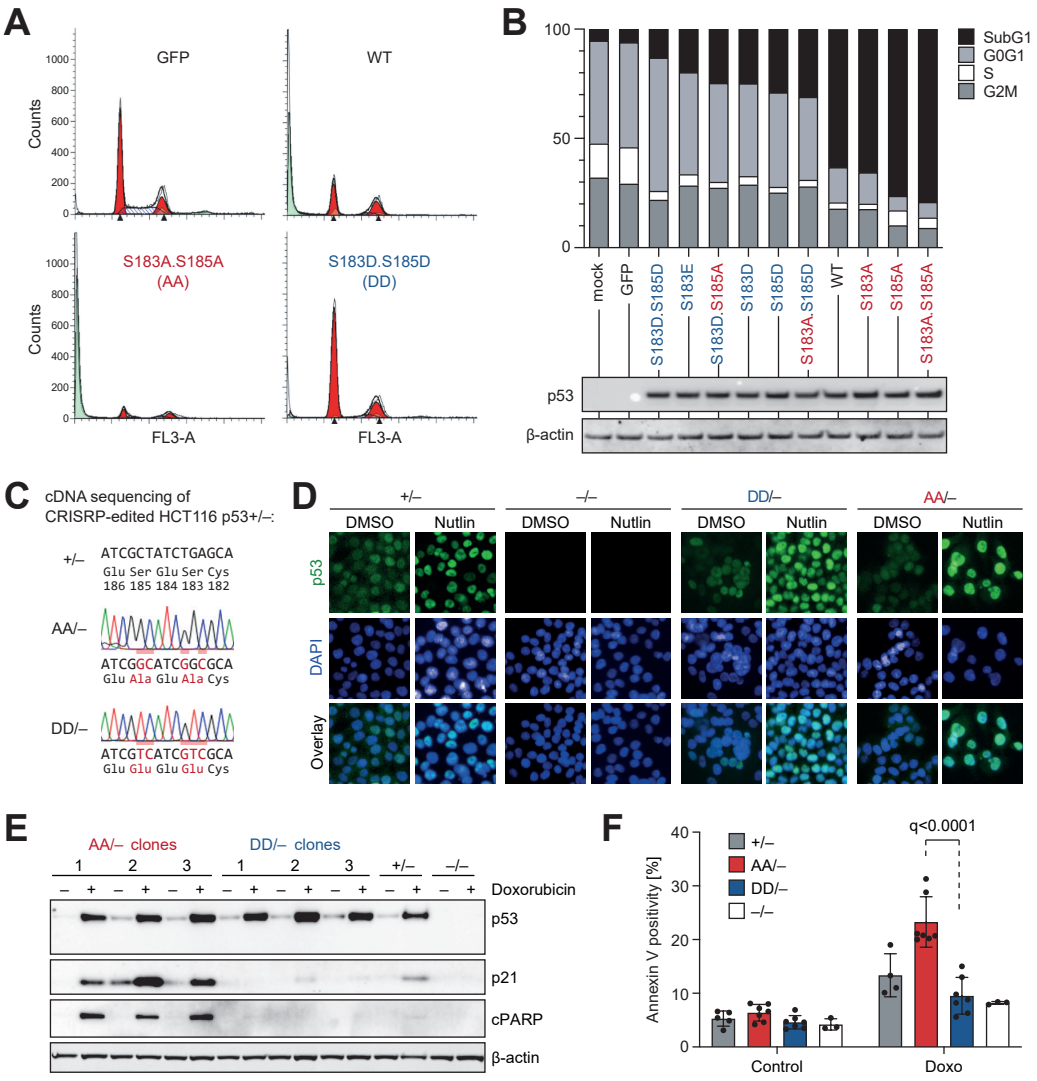

AACR American Association for Cancer Research

Cancer Research

The Journal of Cancer Research (1916–1930) | The American Journal of Cancer (1931–1940)

Phosphorylation control of p53 DNA binding cooperativity balances tumorigenesis and aging

Oleg Timofeev, Lukas Koch, Constantin Niederau, et al.

Cancer Res Published OnlineFirst September 1, 2020.